

## Particulate air quality model predictions using prognostic vs. diagnostic meteorology in central California

Jianlin Hu<sup>a</sup>, Qi Ying<sup>b</sup>, Jianjun Chen<sup>c</sup>, Abdullah Mahmud<sup>c</sup>, Zhan Zhao<sup>a</sup>,  
Shu-Hua Chen<sup>a</sup>, Michael J. Kleeman<sup>c,\*</sup>

<sup>a</sup> Department of Land, Air and Water Resources, University of California, Davis, 1 Shields Ave, Davis CA 95616, USA

<sup>b</sup> Zachry Department of Civil Engineering, Texas A&M University, College Station, TX 77843, USA

<sup>c</sup> Department of Civil and Environmental Engineering, University of California, Davis, 1 Shields Ave, Davis, CA 95616, USA

### ARTICLE INFO

#### Article history:

Received 14 July 2009

Received in revised form

8 October 2009

Accepted 9 October 2009

#### Keywords:

Diagnostic meteorological fields

Prognostic meteorological fields

Data assimilation

UCD/CIT air quality model

California Regional Particulate Air Quality Study (CRPAQS)

### ABSTRACT

Comparisons were made between three sets of meteorological fields used to support air quality predictions for the California Regional Particulate Air Quality Study (CRPAQS) winter episode from December 15, 2000 to January 6, 2001. The first set of fields was interpolated from observations using an objective analysis method. The second set of fields was generated using the WRF prognostic model without data assimilation. The third set of fields was generated using the WRF prognostic model with the four-dimensional data assimilation (FDDA) technique. The UCD/CIT air quality model was applied with each set of meteorological fields to predict the concentrations of airborne particulate matter and gaseous species in central California. The results show that the WRF model without data assimilation over-predicts surface wind speed by ~30% on average and consequently yields under-predictions for all PM and gaseous species except sulfate (S(VI)) and ozone(O<sub>3</sub>). The WRF model with FDDA improves the agreement between predicted and observed wind and temperature values and consequently yields improved predictions for all PM and gaseous species. Overall, diagnostic meteorological fields produced more accurate air quality predictions than either version of the WRF prognostic fields during this episode. Population-weighted average PM<sub>2.5</sub> exposure is 40% higher using diagnostic meteorological fields compared to prognostic meteorological fields created without data assimilation. These results suggest diagnostic meteorological fields based on a dense measurement network are the preferred choice for air quality model studies during stagnant periods in locations with complex topography.

© 2009 Elsevier Ltd. All rights reserved.

### 1. Introduction

Meteorology is a key factor that influences the severity of air pollution events. Air quality models use emissions inventories and meteorological fields to identify the dominant emissions sources that can be controlled to improve air quality. The continuous meteorological fields required by air quality models can be interpolated based on measured data (diagnostic meteorological fields) or they can be generated by global or limited-area weather or climate models (prognostic meteorological fields). Diagnostic fields represent the actual state of the atmosphere at the measurement sites, but their accuracy is often limited by insufficient spatial or temporal measurement density. Diagnostic meteorological fields also lack dynamic consistency among the variables since they are not based on the complete primitive equations (Seaman, 2000).

Prognostic meteorology models have been developed to overcome the shortcomings of diagnostic models. Prognostic models predict values for meteorological variables by solving the atmospheric dynamic equations. Examples of prognostic models include the Penn State University/National Center for Atmospheric Research (PSU/NCAR) Fifth Generation Mesoscale Model (MM5) (Grell et al., 1994), the Colorado State University Regional Atmospheric Modeling System (CSU-RAMS) (Pielke et al., 1992), and the recently-developed Weather Research and Forecasting (WRF) Model (Skamarock et al., 2005; Skamarock and Klemp, 2008). Prognostic models do not require extensive observation networks to generate meteorological fields; however, imperfections in the various physical parameterizations, numerics, and inputs (such as initial and boundary conditions) cause prediction errors. The capability of prognostic models to produce accurate meteorological fields has been improved dramatically through better physical parameterizations, the use of data assimilation methods, and the increased resolution of the horizontal and vertical grid spacing (Seaman, 2003).

\* Corresponding author. Tel.: +1 530 752 8386; fax: +1 530 752 7872.

E-mail address: [mjkleeman@ucdavis.edu](mailto:mjkleeman@ucdavis.edu) (M.J. Kleeman).

Both diagnostic and prognostic meteorological fields have been widely used for air quality modeling studies (Hanna et al., 1996; Hogrefe et al., 2001a,b; Sistla et al., 2001; Jiang and Fast, 2004; Jimenez et al., 2006; Ying et al., 2007, 2008). Diagnostic approaches have successfully represented the meteorology for air quality modeling in the South Coast Air Basin (Mysliwiec and Kleeman, 2002; Ying et al., 2007; Kleeman et al., 2007) and the Central Valley of California (Held et al., 2004; Ying and Kleeman, 2006; Ying et al., 2008). One reason for the persistence of diagnostic models in California is that prognostic models tend to have difficulties simulating accurate meteorological fields in complex topography. Kumar and Russell (1996) studied the performance of the CIT (Carnegie/California Institute of Technology) photochemical air quality model for the Southern California Air Quality Study (SCAQS) with prognostic meteorological fields generated by the fourth PSU/NCAR mesoscale model (MM4) that includes four-dimensional data assimilation (FDDA, Stauffer and Seaman, 1990, 1994; Stauffer et al., 1991) and found that the results were less satisfactory than those obtained using diagnostic fields. Soong et al. (2004) used three sets of prognostic meteorological fields generated by MM5 with different physical configurations and with/without FDDA to drive the Comprehensive Air quality Model with extensions (CAMx) during the Central California Ozone Study (CCOS). Liang et al. (2004) simulated the same CCOS episode using MM5 and the Community Multiscale Air Quality model (CMAQ) and compared the CMAQ results with CAMx results. The performance of both air quality models in the two studies was less than satisfactory. Jackson et al. (2006) tested a hybrid approach to produce meteorological fields for the July/August 2000 CCOS episode. They used the CALMET diagnostic model to improve agreement between MM5 simulated fields and the observed air temperature and wind speed and found that the hybrid meteorological fields generated better ozone predictions for central California than MM5 fields alone. Pun et al. (2009) conducted PM simulations using the MM5 meteorological model and the Community Multiscale Air Quality model with the Model of Aerosol Dynamics, Reaction, Ionization, and Dissolution (CMAQ/MADRID) for a subset (December 25th–December 31st, 2000) of the CRPAQS episode. Average MM5 prognostic wind speeds were over-predicted by  $0.73 \text{ m s}^{-1}$  and the average surface temperatures were over-predicted by 2 K, leading to a  $\sim 35\%$  over-prediction for 24-h average PM nitrate concentration and a  $\sim 22\%$  under-prediction for 24-h average total  $\text{PM}_{2.5}$  mass.

The purpose of this study is to evaluate the air quality model performance for the full CRPAQS 2000–2001 winter episode (December 15th, 2000–January 6th, 2001) driven by three different sets of meteorological fields. The first set of fields was generated by a diagnostic meteorological model based on measurements using the objective analysis method. The second and third sets of fields were generated using the prognostic WRF model with and without FDDA, respectively. The UCD/CIT air quality model was applied to predict the concentrations of gaseous and particle species using each of the meteorological fields in turn. Model predictions for PM species were then compared to ambient measurements in the heavily polluted San Joaquin Valley (SJV).

## 2. Model description

The UCD/CIT air quality model used in the present study is based on the CIT airshed model (McRae et al., 1982; Harley et al., 1993). A detailed description of the UCD/CIT model and the history of its evolution have been presented in previous studies (Kleeman et al., 1997; Kleeman and Cass, 2001; Mysliwiec and Kleeman, 2002; Ying and Kleeman, 2003, 2006; Held et al., 2004; Ying et al., 2008), so only the aspects that were changed during the current study are discussed here. The UCD/CIT air quality model was revised for the

current project to be compatible with both prognostic wind fields (C-grid) and diagnostic wind fields (A-grid). Previous studies (Byun, 1999; Odman and Russell, 2000; Lee et al., 2004; Hu et al., 2006; Sportisse et al., 2007) have discussed the occurrence of mass consistency errors when the meteorological model and the chemistry-transport model do not use the same grid system, the same interpolation strategies and/or the same transport algorithms. Two correction methods are commonly used in air quality models to overcome this problem. The first correction method transports a uniform tracer along with other species so that concentrations can be re-normalized after each time step. The second correction method directly adjusts the vertical wind velocity within the framework of the air quality model in order to satisfy mass consistency. Hu et al. (2006) examined both correction methods using MM5 and CMAQ and proved that adjusting the vertical wind velocity is an effective method to conserve mass. Recalculation of vertical winds was therefore incorporated into the UCD/CIT framework. The approach for gas–particle transfer of inorganic species was updated in the current study to increase the model speed. The vapor pressure of semi-volatile inorganic species above each particle surface was calculated based on ISORROPIA II (<http://nenes.eas.gatech.edu/ISORROPIA>; Nenes et al., 1998; Fountoukis and Nenes, 2007). Gas–particle mass transfer was calculated based on the solution to the dynamic equations developed by Jacobson (2005). The combination of these changes increases the speed of model calculations by roughly a factor of two. Other aspects of the UCD/CIT reactive chemical transport model (e.g., gas-phase mechanism, advection scheme, deposition scheme, and secondary organic aerosol calculation, etc.) have been described by Ying et al. (2008), and are not repeated here.

## 3. Model application

Three sets of simulations were conducted in the current study using one set of diagnostic meteorological fields and two sets of prognostic meteorological fields. Each of the simulations predicted air quality in California's central valley from December 15th, 2000 to January 6th, 2001. The model domain (see Fig. 6) has  $95 \times 95 \times 10$  grid cells (xyz), with a horizontal resolution of 8 km and vertical layers up to 5 km. The thickness of each vertical layer starting from the surface is 35, 105, 140, 330, 390, 500, 500, 1000, 1000, and 1000 m.

### 3.1. Diagnostic meteorological fields

A detailed description of the diagnostic meteorological fields is provided by Ying et al. (2008) and so only a brief description of the diagnostic methods are summarized here. The diagnostic 3D temperature, humidity and wind fields were interpolated from surface and vertical meteorological measurements using the objective analysis method described by Goodin et al. (1979, 1980). Hourly surface measurements of wind (120 stations), humidity (132 stations) and temperature (192 stations) were collected throughout the portion of the modeling domain over land. Hourly vertical wind and virtual temperature profiles were collected at 20 stations during the entire study period. Balloon soundings of relative humidity at Oakland, Fresno, and Bakersfield were measured four times a day on December 15–18, December 26–28, 2000, and January 4–7, 2001. The humidity measurements were linearly interpolated temporally to generate hourly humidity inputs for the objective analysis program. For the days without humidity measurement, the nearest day was taken as a surrogate day for the humidity fields. There were no observations of wind, temperature, and humidity over the Pacific Ocean. The results from a MM5 simulation performed by staff at the California Air Resources Board

(CARB) were used as surrogate observations at 17 virtual stations to provide the best possible estimate of meteorological conditions. There were no background model fields used over land area. The Noilhan and Planton land-surface parameterization scheme (Noilhan and Planton, 1989) was used to estimate the sensible and latent heat flux from the ground. Equation 6.18 on page 155 in Garratt's book (Garratt, 1994) was then applied to calculate the development of the convective mixing layer height during the day. The mixing height at night was believed to be low due to radiative cooling of the surface and was fixed at 50 m. The convective mixing layer was assumed to collapse immediately after the sun went down (solar zenith angle > 85°).

3.2. Prognostic meteorological fields

Two sets of prognostic fields were generated with version 2.2 of the Advanced Research WRF (ARW) model using 3 nested domains (2-way interaction with feedback) that had horizontal resolutions of 36, 12, and 4 km, respectively. The first WRF simulation did not employ any data nudging while the second WRF simulation employed the observation nudging technique in all three domains at all model levels for temperature, moisture, and wind, and employed

the reanalysis nudging in the 36-km domain above the boundary layer. All WRF simulations were configured with the Thompson graupel microphysics scheme (Thompson et al., 2004), Monin–Obukhov surface layer scheme (Skamarock et al., 2005), Noah land-surface model (Chen and Dudhia, 2001), and Yonsei University (YSU, Hong et al., 2006) boundary layer scheme. This optimal configuration was chosen based on a study conducted by Zhan et al. (in preparation) in which various WRF configurations were tested for conditions in central California. The 4 km meteorological fields generated by the WRF model were then averaged to 8 km to produce the inputs for air quality modeling. It is commonly believed that finer grid size in meteorology simulation provides a better description of small-scale dynamics (e.g., land–sea breezes and orographical winds). The combination of 4 km meteorological simulations and 8 km air quality simulations yields an efficient combination of the models without significant loss of accuracy. Finer resolutions have shown to improve air quality predictions (Hass et al., 1997); however, other studies have found that (beyond a certain point) finer grid resolution does not necessarily yield better air quality predictions (Menut et al., 2005). One possible explanation for this finding is that the current generation of first-order turbulence closure schemes employed in regional air quality models are

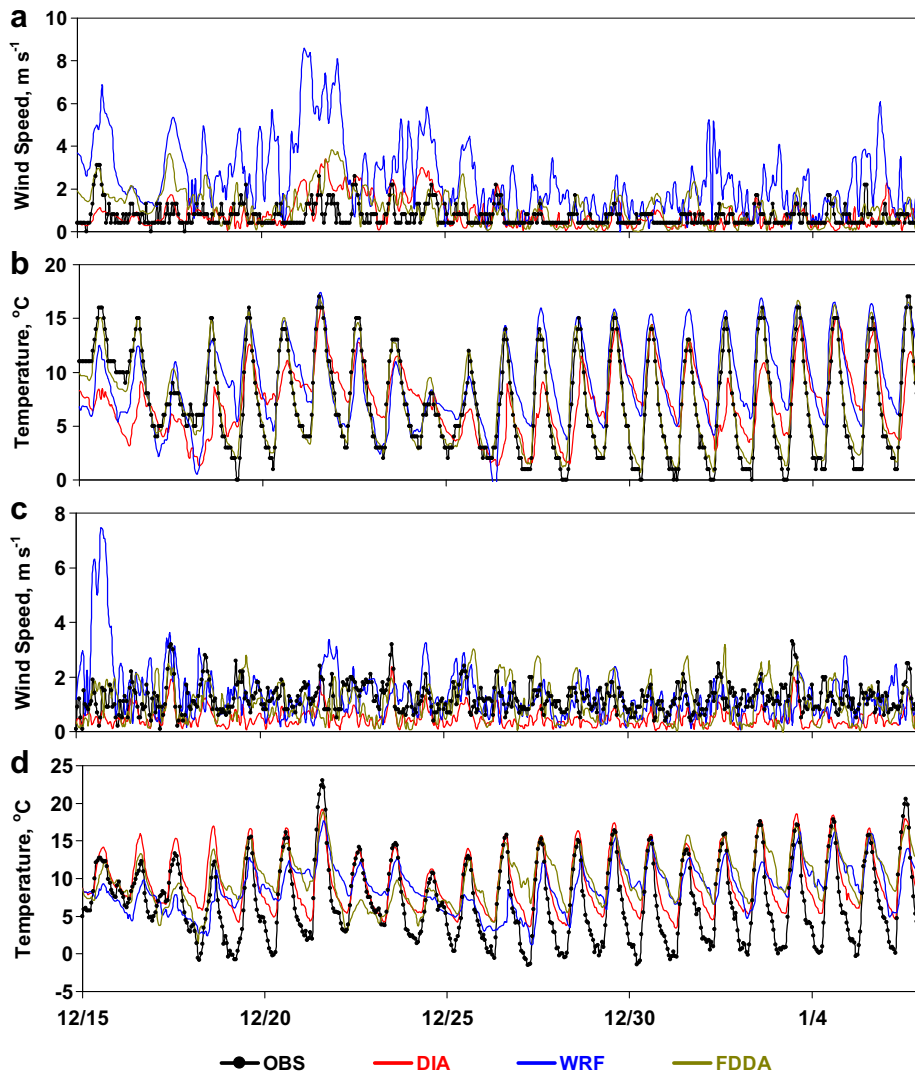


Fig. 1. Time series of ground-level observed and simulated (a) wind speed and (b) temperature at the Fresno station; and (c) wind speed and (d) temperature at the Famoso station near Bakersfield (about 30 km north of Bakersfield).

**Table 1**

Statistics of meteorology parameters in DIA, WRF and FDDA meteorology. RMSE and MAE are the root mean squared error and the mean absolute error, respectively.

Meteorological field		Domain			SJV		
		Mean	RMSE	MAE	Mean	RMSE	MAE
Temp (°C)	Obs	8.8	—	—	6.9	—	—
	DIA	9.1	3.2	2.5	8.4	3.1	2.4
	WRF	8.4	5.0	4.0	8.1	5.1	4.1
	FDDA	10.3	4.8	3.8	9.7	5.0	4.0
RH (%)	Obs	65.7	—	—	73.2	—	—
	DIA	59.0	18.9	15.1	60.0	20.7	17.3
	WRF	63.4	24.7	19.3	65.0	22.8	17.8
	FDDA	55.3	25.0	19.7	62.1	23.5	18.4
U_wind	Obs	1.22	—	—	0.72	—	—
	DIA	1.12	1.58	0.92	0.67	0.67	0.48
	WRF	1.52	1.86	1.30	1.25	1.18	0.84
	FDDA	1.33	1.61	1.06	0.87	1.07	0.70
V_wind	Obs	1.22	—	—	0.78	—	—
	DIA	1.13	1.47	0.88	0.70	0.77	0.52
	WRF	1.67	1.88	1.34	1.01	1.10	0.78
	FDDA	1.45	1.69	1.10	0.69	0.98	0.67

effectively tuned for a grid resolution of 4–5 km. Ying et al. (2008) studied the effects of horizontal resolution on air quality model predictions during the winter CRPAQS study and found that the model predictions using 4 km and 8 km resolution generally agree with one another except that the coarser resolution leads to slightly lower concentrations of primary pollutants near emission sources by distributing the emissions evenly in the coarser cell.

### 3.3. Other inputs

All three simulations carried out in current study used the emissions inventory, initial and boundary conditions and other inputs described by Ying et al. (2008).

## 4. Results and discussion

The general synoptic pattern during CRPAQS 2000 winter episode was strong high pressure aloft positioned along the West Coast providing a general area of subsidence and stable meteorological conditions over the SJV. High pressure gradually intensified

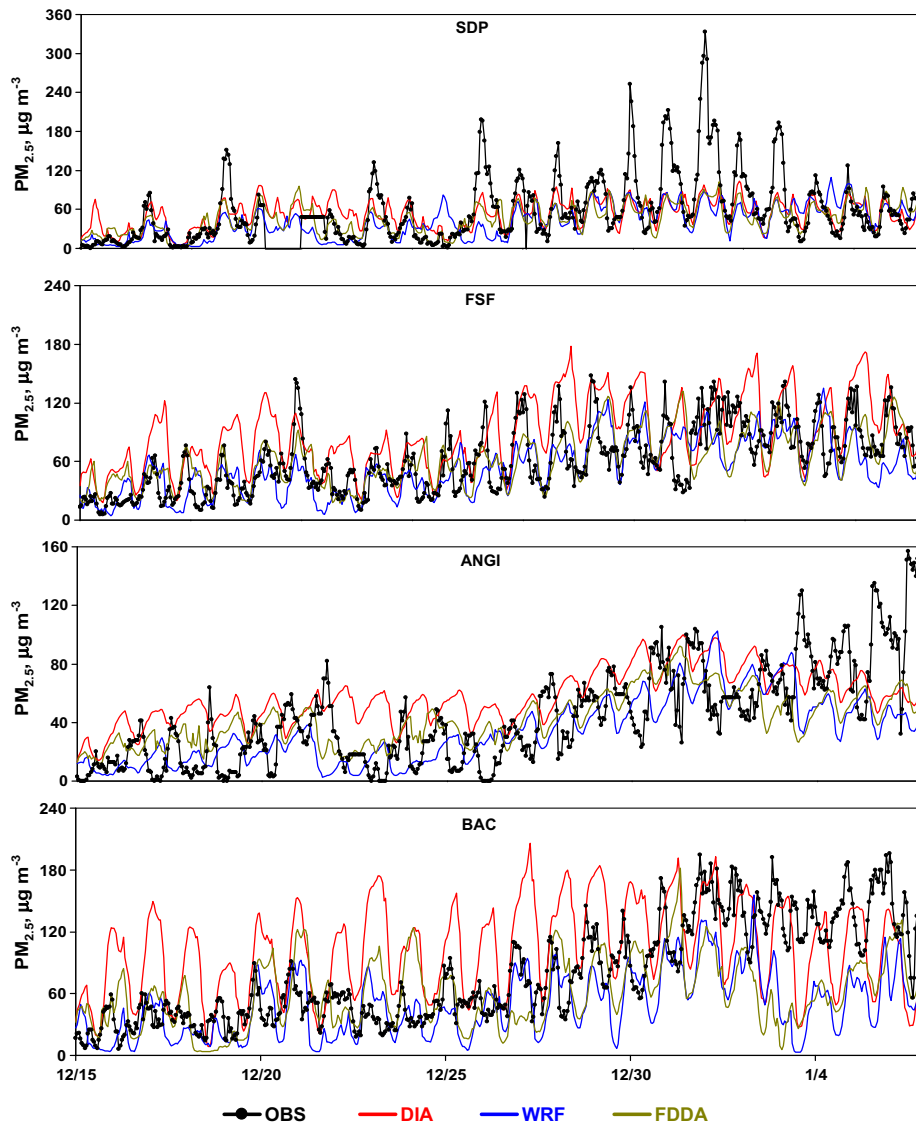


**Fig. 2.** Time series of  $PM_{2.5}$  mass concentration at Sacramento (SDP), Fresno (FSF), Angiola (ANGI), and Bakersfield (BAC) during December 2000 and January 2001 generated with diagnostic (DIA), WRF-simulated (WRF), and WRF-FDDA simulated (FDDA) meteorology.

over SJV from December 12th to 20th. A weak upper level disturbance briefly broke down the ridge on December 24th, which slightly improved the dispersion conditions. After this weak trough passage, the high pressure rebuilt and stable meteorological conditions continued through the end of the episode on January 7th, 2001. Fig. 1 illustrates the time series of ground-level wind speed and temperature measured during the CRPAQS episode (OBS), generated by the diagnostic interpolation method (DIA), simulated by WRF model with no data assimilation (WRF), and simulated by the WRF model with the FDDA technique (FDDA) for all hours at Fresno and Famoso (about 30 km north of Bakersfield). The results reveal that the DIA and FDDA wind speed are in excellent agreement with observations, while WRF predictions with no data assimilation overestimate the surface wind. The predicted and observed diurnal variation of temperature is also in excellent agreement, but the WRF prognostic temperature is greater than observations at night and lower than observations during the day, especially at the Famoso station. FDDA improves the WRF daytime temperature predictions significantly at Fresno and Famoso. FDDA also improves nighttime temperature predictions at Fresno but nighttime temperature is still over-predicted at Famoso.

Table 1 presents root mean squared errors (RMSE) and mean absolute errors (MAE) summarizing the comparison between the observed and simulated meteorological parameters of interest for air pollution modeling using all observations in the entire modeling domain and in SJV, respectively. The average measured surface wind components in the entire domain are  $U = 1.2$  and  $V = 1.2 \text{ m s}^{-1}$ ; with slightly smaller values of  $U = 0.72$  and  $V = 0.78 \text{ m s}^{-1}$  in SJV. This low surface wind speed reflects very stagnant conditions during the CRPAQS episode. The diagnostic method slightly under-predicts the wind speeds, resulting in  $RMSE_U = 1.58 \text{ m s}^{-1}$  and  $RMSE_V = 1.47 \text{ m s}^{-1}$  in the entire domain, and  $RMSE_U = 0.67 \text{ m s}^{-1}$  and  $RMSE_V = 0.77 \text{ m s}^{-1}$  in the SJV. WRF with no data assimilation tends to over-predict the mean wind speed by 30% with  $RMSE_U = 1.86 \text{ m s}^{-1}$  and  $RMSE_V = 1.88 \text{ m s}^{-1}$  in the entire domain, and  $RMSE_U = 1.18 \text{ m s}^{-1}$  and  $RMSE_V = 1.10 \text{ m s}^{-1}$  in the SJV. WRF with data assimilation slightly over-predicts the mean wind speed by 10% with  $RMSE_U = 1.61 \text{ m s}^{-1}$  and  $RMSE_V = 1.69 \text{ m s}^{-1}$  in the entire domain but performs better in the SJV with  $RMSE_U = 1.07 \text{ m s}^{-1}$  and  $RMSE_V = 0.98 \text{ m s}^{-1}$ . The mean observed temperature and relative humidity across the entire domain is  $8.8 \text{ }^\circ\text{C}$  and 65.7%, respectively. Diagnostic temperature is

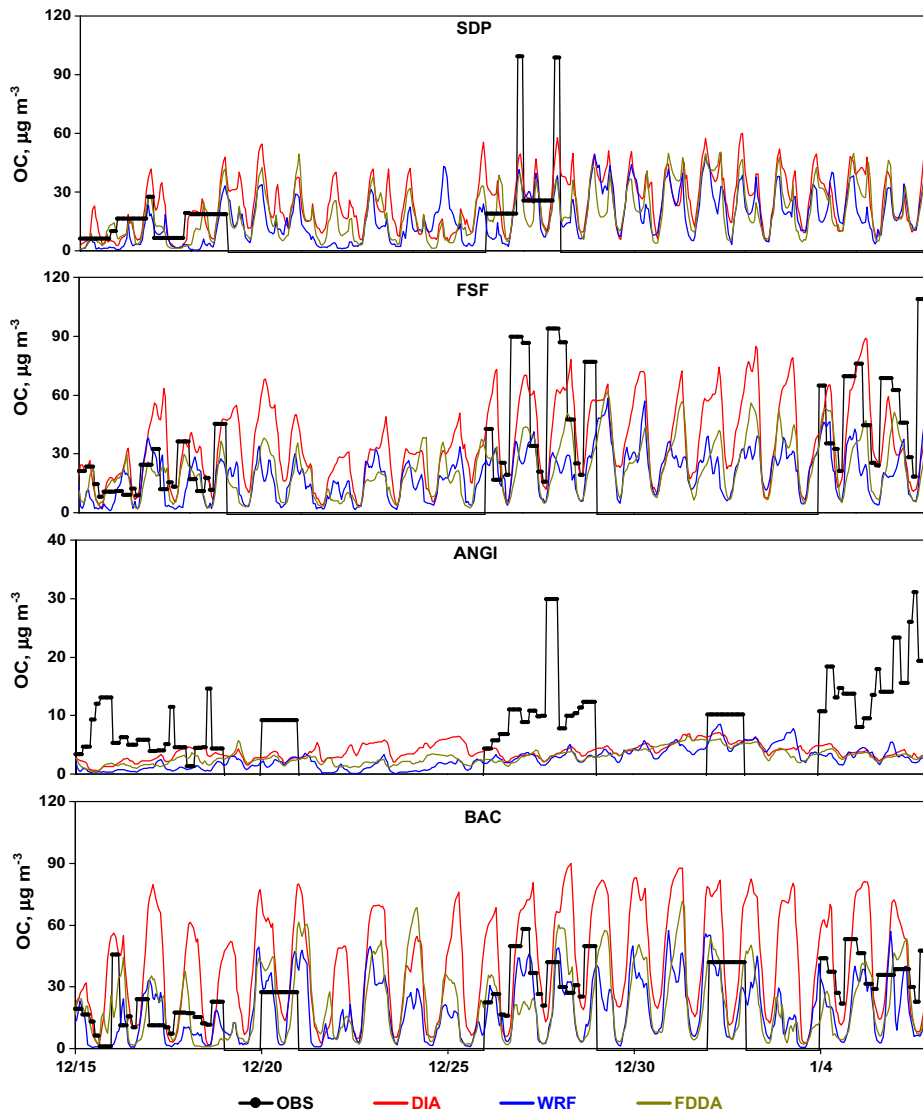


Fig. 3. Time series of OC concentration at Sacramento (SDP), Fresno (FSF), Angiola (ANGI), and Bakersfield (BAC) during December 2000 and January 2001 generated with diagnostic (DIA), WRF-simulated (WRF), and WRF-FDDA simulated (FDDA) meteorology.

0.3 °C higher than observations with a RMSE of 3.2 °C. Although WRF with no data assimilation under-predicts daytime temperature and over-predicts nighttime temperature (as shown in Fig. 1), the average temperature is 0.4 °C lower than observations with an RMSE of 5.0 °C. The average WRF-FDDA temperature is 1.5 °C higher than observations but with a slightly lower RMSE of 4.8 °C, because FDDA leads to relatively accurate predictions for daytime temperature, but nighttime temperatures are still over-predicted. Domain-wide average relative humidity predicted by the Diagnostic, WRF and FDDA models is lower than observation by a RMSE of 18.9%, 24.7% and 25.0%, respectively. The higher temperature predicted by the WRF-FDDA model leads to lower relative humidity compared to the other models. Trends for temperature and humidity in the SJV are similar to those observed for the entire domain.

Fig. 2 illustrates a comparison between ambient measurements of PM<sub>2.5</sub> mass concentration and predicted PM<sub>2.5</sub> generated with the diagnostic and prognostic meteorology fields. Comparisons are made at four central valley stations: Sacramento (SDP), Fresno (FSF), Angiola (ANGI) and Bakersfield (BAC), arranged from north to south. SDP, FSF, and BAC are the three major urban sites in the central valley while ANGI is a rural site. Overall, the air quality

predictions made using any of the prognostic or diagnostic meteorological fields capture the increased PM<sub>2.5</sub> concentrations during the evening hours at the urban sites due to the effects of decreased vertical mixing and increased emissions mostly from wood combustion at night (Ying et al., 2008). PM<sub>2.5</sub> predictions generated using the diagnostic fields are generally higher than the predictions generated with the WRF and FDDA prognostic fields because diagnostic fields exhibit lower mixing depths and lower wind speeds leading to less dilution. All three predictions are reasonably close to observations for most days during the episode at the SDP site, but they all under-predict the peak values between December 30th, 2000 and January 3rd, 2001, which indicates a likely emissions under-estimation or an under-prediction of secondary PM formation on these days. FDDA prognostic PM<sub>2.5</sub> predictions are in excellent agreement with observations at the FSF site, while the diagnostic PM<sub>2.5</sub> predictions are 40% higher than measurements and WRF prognostic PM<sub>2.5</sub> predictions are 18% lower than measurements. At the BAC site, the differences between the diagnostic and prognostic meteorology fields cause even more noticeable changes in PM<sub>2.5</sub> predictions: diagnostic PM<sub>2.5</sub> predictions are significantly higher than measured values from December 15th to

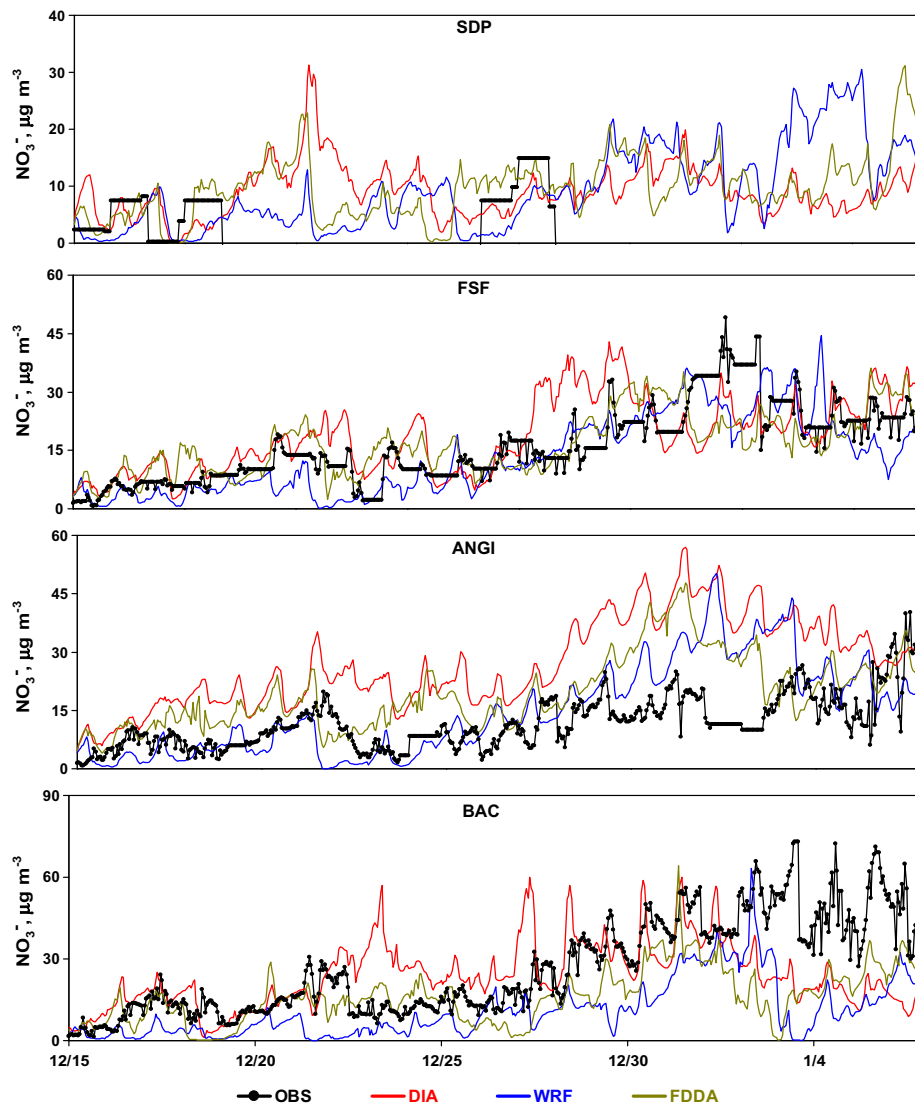


Fig. 4. Time series of N(V) mass concentration at Sacramento (SDP), Fresno (FSF), Angiola (ANGI), and Bakersfield (BAC) during December 2000 and January 2001 generated with diagnostic (DIA), WRF-simulated (WRF), and WRF-FDDA simulated (FDDA) meteorology.

29th and lower than measured values from January 2nd to 6th. Both WRF and FDDA prognostic PM<sub>2.5</sub> predictions are in good agreement with measured values from December 15th to 28th, but significantly lower than measured values for the rest of the episode. The differences between diagnostic and prognostic predictions at this foothills site are much larger than at other sites, reflecting the difficulty in simulating small-scale circulations generated by the complex terrain. At the rural ANGI site, the diagnostic and prognostic PM<sub>2.5</sub> predictions have similar diurnal patterns, but none of the model predictions match the observed diurnal pattern. All three predictions miss the high PM<sub>2.5</sub> concentrations at the end of the episode (January 3rd–6th), but have a reasonably good agreement with observations from December 15th to January 2nd.

Fig. 3 shows the measured and predicted particulate organic carbon (OC) concentrations at SDP, FSF, ANGI and BAC. Winter OC at urban locations in the SJV is mainly associated with primary sources (Ying et al., 2008) and so the prognostic vs. diagnostic predictions follow expected trends based on different amounts of dilution acting on the same emissions. Overall, OC concentrations are significantly under-predicted using all three versions of the meteorological fields. WRF and WRF-FDDA prognostic OC predictions are even lower than diagnostic predictions due to the higher mixing depth and higher wind speed in the prognostic meteorological fields. Diagnostic and prognostic OC predictions at the SDP site have similar values. OC predictions from December 15th to 18th are in good agreement with observed concentrations, while predicted OC concentrations are 2–3 times lower than the observed concentrations on December 26th and 27th. At the FSF site, diagnostic OC predictions are in a reasonably good agreement with measured

values while WRF and FDDA prognostic OC predictions are lower than the observations. In contrast, diagnostic OC predictions at the BAC urban site are higher than measurements while WRF and FDDA prognostic OC predictions are in reasonable agreement with the measured values. At the rural ANGI site, both diagnostic and prognostic OC predictions are lower than the measured concentrations, possibly due to missing emissions (Ying et al., 2008) or due to an under-prediction of secondary organic aerosol (SOA) formation in the rural environment where SOA becomes an important source of OC (Chen et al., in press).

Fig. 4 shows the measured and predicted PM nitrate (N(V)) concentrations at SDP, FSF, ANGI and BAC. Both measured and predicted N(V) concentrations have less of a diurnal cycle than OC, with a gradual buildup observed throughout the episode as NO<sub>x</sub> is slowly converted to nitric acid by ozone (Ying et al., 2008). N(V) production involves transport of both gas-phase and particle-phase reactive nitrogen species and their chemical conversion to particulate nitrate. Overall WRF and FDDA prognostic N(V) predictions are lower than diagnostic N(V) predictions, yielding a trend similar to that for PM<sub>2.5</sub> mass and particulate OC. The diagnostic and FDDA prognostic N(V) predictions at SDF and FSF are in a good agreement with measured values, while the WRF prognostic N(V) predictions are generally lower than measured values at the urban sites and higher at the rural site. It should be noted that the continuous N(V) measurements at FSF, ANGI, and BAC are lower than filter-based N(V) measurements at those sites, suggesting that the continuous measurements may be biased low.

Table 2 shows the calculated mean fractional bias (MFB) for PM<sub>2.5</sub>, N(V), ammonium ion (N(-III)), S(VI), elemental carbon (EC),

**Table 2**  
Mean fractional biases of PM and gas species.

SITE		ANGI	BAC	BTI	FSF	SNFH	M14	SDP	DAV	BODB <sup>a</sup>	SEQU <sup>b</sup>	OVERALL
PM <sub>2.5</sub>	DIA	0.44	0.31	0.37	0.39	-0.60	-	0.16	-	-	-	0.19
	WRF	-0.15	-0.47	-0.18	-0.13	-0.67	-	-0.20	-	-	-	-0.30
	FDDA	0.17	-0.22	0.10	0.08	-0.55	-	-0.01	-	-	-	-0.07
N(V)	DIA	0.83	0.01	0.98	0.21	-0.15	0.08	-0.03	0.47	0.62	-1.08	0.23
	WRF	0.04	-0.89	0.40	-0.29	-0.34	-0.57	-0.60	0.24	0.05	-0.89	-0.30
	FDDA	0.53	-0.43	0.71	0.12	-0.12	-0.13	0.03	0.04	0.36	-0.65	0.08
N(-III)	DIA	-0.66	-0.16	0.62	-0.58	-0.19	-0.05	0.02	-0.14	1.06	0.02	0.01
	WRF	-1.12	-0.79	0.10	-1.00	-0.32	-0.61	-0.42	-0.14	0.66	-0.05	-0.38
	FDDA	-0.85	-0.57	0.48	-0.73	-0.11	-0.24	0.12	-0.48	0.92	0.11	-0.12
S(VI)	DIA	0.14	0.48	0.84	0.65	0.58	0.44	0.54	0.96	0.05	0.50	0.48
	WRF	-0.06	-0.07	0.75	0.27	0.54	0.06	0.33	0.93	-0.02	0.48	0.27
	FDDA	0.05	0.05	0.86	0.42	0.60	0.24	0.48	1.02	-0.09	0.51	0.36
EC	DIA	-0.10	0.18	-0.02	0.05	-0.77	0.58	0.73	0.63	0.17	-0.90	-0.06
	WRF	-0.58	-0.71	-0.57	-0.71	-0.84	-0.11	0.11	0.20	-0.73	-1.00	-0.59
	FDDA	-0.29	-0.60	-0.23	-0.47	-0.74	0.25	0.52	0.47	-0.44	-0.82	-0.35
OC	DIA	-0.89	0.20	-0.25	-0.08	-1.28	-0.05	-0.13	-0.60	-0.89	-1.66	-0.62
	WRF	-1.20	-0.63	-0.80	-0.73	-1.36	-0.79	-0.80	-1.01	-1.44	-1.68	-1.08
	FDDA	-1.07	-0.48	-0.50	-0.54	-1.29	-0.50	-0.40	-0.87	-1.24	-1.61	-0.89
O <sub>3</sub>	DIA	0.56	-0.29	-0.01	-0.32	0.23	-0.01	0.05	0.04	0.68	0.25	0.09
	WRF	0.55	0.07	0.36	-0.06	0.28	0.15	0.24	0.47	0.80	0.47	0.33
	FDDA	0.62	-0.01	0.19	-0.11	0.26	0.16	0.17	0.38	0.95	0.25	0.29
NO	DIA	-1.14	0.23	-0.38	0.07	-0.61	-0.38	-0.20	-0.05	-0.97	-0.72	-0.22
	WRF	-1.47	-0.73	-0.83	-0.65	-0.08	-1.09	-0.63	-0.88	-1.20	-1.15	-0.76
	FDDA	-1.25	-0.50	-0.82	-0.49	-0.31	-0.92	-0.46	-0.78	-1.16	-0.88	-0.62
NO <sub>2</sub>	DIA	0.09	0.24	-0.05	0.25	-0.88	0.19	0.49	0.50	0.16	0.05	0.21
	WRF	-0.07	-0.24	-0.44	-0.15	-0.98	-0.18	0.18	-0.05	-0.24	-0.18	-0.25
	FDDA	-0.03	-0.17	-0.28	-0.10	-0.77	-0.03	0.32	0.07	-0.12	-0.06	-0.21
CO	DIA	-	0.10	0.04	0.03	-	-0.09	0.18	0.48	-0.45	-0.29	0.07
	WRF	-	-0.36	-0.14	-0.38	-	-0.32	-0.05	0.24	-0.69	-0.46	-0.17
	FDDA	-	-0.30	-0.09	-0.33	-	-0.22	0.03	0.28	-0.66	-0.38	-0.12

<sup>a</sup> Site SRF for gas species, 33.9 km to BODB.

<sup>b</sup> Site VCS for gas species, 44.7 km to SEQU.

OC, and gas-phase O<sub>3</sub>, NO, NO<sub>2</sub>, and CO at 10 sites and the domain average using all available measurements. There are no observations for gas species O<sub>3</sub>, NO, NO<sub>2</sub>, and CO at sites BODB and SEQU and so the measurements from nearby sites (SRF and VCS) are used instead. Model calculations driven by the diagnostic meteorology tend to over-predict PM species except OC. FDDA prognostic meteorology yields excellent predictions for N(V) and total PM<sub>2.5</sub> mass, but under-predicts all other species except S(VI) and O<sub>3</sub>. Model calculations driven by WRF prognostic meteorology under-predict all species except S(VI) and O<sub>3</sub> at most of the sites due to higher wind speeds and mixing depths. OC is consistently under-predicted at most of the sites by a factor of 2 or more, with an overall MFB  $-0.62$  to  $-1.08$ . O<sub>3</sub> concentrations during this cold winter episode were controlled by transport of background ozone to the surface, followed by dry deposition and chemical losses. Therefore, WRF and FDDA prognostic meteorology fields yield higher ground-level O<sub>3</sub> concentrations than the diagnostic fields due to strong mixing among vertical layers which transports the background O<sub>3</sub> from upper layers to the surface. WRF and FDDA prognostic NO concentrations are also significantly under-predicted with an overall MFB of  $-0.90$  and  $-0.88$ , respectively. Along with increased dilution due to high wind speeds and mixing depth, prognostic NO is also consumed by higher ground-level O<sub>3</sub> concentrations via titration. Overall, the diagnostic meteorology leads to better agreement with the observed concentrations, with most of the overall MFB less than 0.3; WRF meteorology yields lower concentrations, but nudging with observed meteorology improves the model predictions, even though FDDA still yields relatively large bias for certain species. Additional analysis of the diagnostic model predictions has been provided by [Ying et al. \(2008\)](#).

While MFB quantifies the average tendency of model predictions, mean fraction error (MFE) illustrates the average difference between the model predictions and the measured concentrations. [Table 3](#) summarizes the MFE calculated for the six PM and four gas-phase species. Prognostic and diagnostic MFE values are not statistically different, indicating that the prognostic model predictions are as good as the diagnostic predictions in terms of the absolute difference between the predictions and the observations ([Table 3](#)). [Boylan and Russell \(2006\)](#) recommended performance criteria of  $\pm 0.60$  for MFB and 0.75 for MFE for PM modeling when the observed concentrations are above  $2.25 \mu\text{g m}^{-3}$ . The current model applications meet these criteria for hourly PM<sub>2.5</sub> and all its components except for OC. These results are consistent with [Pun et al. \(2009\)](#).

[Fig. 5\(a\)](#) and [\(b\)](#) illustrates the overall MFB calculated for the SJV and the entire modeling domain, respectively. In the SJV, the UCD/CIT model with the diagnostic meteorology slightly over-predicts concentrations of all species except for O<sub>3</sub>, N(–III), EC and OC, while the same model using WRF prognostic meteorology tends to under-predict all species except for O<sub>3</sub> and S(VI). WRF under-predictions are largest for OC, EC and NO. WRF-FDDA meteorology improves air quality model predictions for almost all species. Average trends across the entire modeling domain are similar to those observed in the SJV, but the magnitude of the MFB is reduced. For example, the MFB of the WRF prognostic N(V) and N(–III) averaged across the entire domain are  $-0.30$  and  $-0.38$ , respectively; while in the SJV, they are  $-0.49$  and  $-0.73$ , respectively. The greater under-prediction of WRF prognostic N(V) and N(–III) in the SJV reflects the influence of high wind speeds in the prognostic meteorology that transports the pollutants out of the valley.

**Table 3**  
Mean fractional errors of PM and gas species.

SITE		ANGI	BAC	BTI	FSF	SNFH	M14	SDP	DAV	BODB <sup>a</sup>	SEQU <sup>b</sup>	OVERALL
PM <sub>2.5</sub>	DIA	0.63	0.57	0.58	0.50	0.91	–	0.55	–	–	–	0.62
	WRF	0.68	0.67	0.62	0.43	0.89	–	0.66	–	–	–	0.65
	FDDA	0.57	0.61	0.47	0.38	0.74	–	0.52	–	–	–	0.54
N(V)	DIA	0.83	0.53	1.04	0.41	1.07	0.72	0.70	0.74	0.82	1.08	0.70
	WRF	0.62	0.92	0.85	0.48	0.89	0.78	1.10	1.22	0.78	0.93	0.79
	FDDA	0.61	0.62	0.94	0.39	0.67	0.64	0.58	1.07	0.77	0.86	0.68
N(–III)	DIA	0.76	0.52	0.72	0.62	0.71	0.67	0.71	0.41	1.20	0.41	0.70
	WRF	1.17	0.81	0.66	1.01	0.66	0.76	0.89	0.86	1.16	0.48	0.84
	FDDA	0.88	0.67	0.65	0.75	0.46	0.59	0.52	0.59	1.11	0.49	0.69
S(VI)	DIA	0.51	0.66	0.88	0.69	0.59	0.60	0.54	0.96	0.43	0.56	0.62
	WRF	0.46	0.43	0.80	0.43	0.57	0.49	0.46	0.94	0.46	0.54	0.53
	FDDA	0.43	0.48	0.90	0.48	0.59	0.54	0.50	1.03	0.48	0.56	0.57
EC	DIA	0.50	0.52	0.51	0.37	0.78	0.78	0.81	0.68	0.72	0.68	0.66
	WRF	0.69	0.82	0.72	0.76	0.85	0.62	0.78	0.46	1.16	0.98	0.81
	FDDA	0.52	0.78	0.56	0.60	0.75	0.66	0.75	0.53	0.85	0.87	0.70
OC	DIA	0.93	0.63	0.45	0.49	1.28	0.47	0.57	0.61	0.89	1.66	0.85
	WRF	1.21	0.76	0.82	0.86	1.36	0.84	0.93	1.01	1.44	1.68	1.12
	FDDA	1.10	0.82	0.58	0.70	1.29	0.61	0.63	0.87	1.24	1.61	0.98
O <sub>3</sub>	DIA	0.67	0.57	0.67	0.59	0.33	0.57	0.57	0.54	1.06	0.51	0.69
	WRF	0.71	0.60	0.71	0.71	0.40	0.76	0.68	0.73	1.10	0.75	0.72
	FDDA	0.74	0.64	0.68	0.60	0.37	0.69	0.61	0.61	1.14	0.59	0.69
NO	DIA	1.15	0.62	0.86	0.67	0.61	0.84	0.75	0.77	1.18	0.93	0.93
	WRF	1.48	0.96	1.11	0.97	0.08	1.18	0.95	1.23	1.30	1.22	1.13
	FDDA	1.25	0.89	0.97	0.81	0.40	1.04	0.82	1.03	1.25	1.03	1.04
NO <sub>2</sub>	DIA	0.66	0.47	0.46	0.41	0.97	0.41	0.52	0.59	0.50	0.48	0.64
	WRF	0.70	0.54	0.64	0.37	1.02	0.46	0.47	0.65	0.53	0.45	0.71
	FDDA	0.63	0.52	0.53	0.39	0.90	0.40	0.44	0.51	0.53	0.43	0.68
CO	DIA	–	0.42	0.28	0.40	–	0.65	0.63	0.53	0.53	0.47	0.52
	WRF	–	0.58	0.33	0.55	–	0.66	0.68	0.46	0.73	0.51	0.57
	FDDA	–	0.58	0.26	0.51	–	0.62	0.66	0.43	0.70	0.47	0.55

<sup>a</sup> Site SRF for gas species, 33.9 km to BODB.

<sup>b</sup> Site VCS for gas species, 44.7 km to SEQU.

Fig. 6 compares the concentrations of (1) diagnostic, (2) WRF, and (3) FDDA prognostic (A) PM<sub>2.5</sub>, (B) N(V), (C) N(-III), (D) S(VI), (E) EC, and (F) OC averaged over the entire episode. All three predictions exhibit a similar spatial distribution of PM species, with high concentrations throughout the SJV, especially at the cells around urban area (e.g., Bakersfield, Fresno, etc.). The diagnostic meteorology yields the highest PM<sub>2.5</sub> concentration, while the WRF prognostic meteorology generates the lowest PM<sub>2.5</sub> concentration throughout the domain, mainly due to the effects of higher wind speeds and larger mixing depth in prognostic meteorology fields. The FDDA meteorology predicts a median concentration of PM<sub>2.5</sub>, reflecting the influence of observed wind speeds on the model predictions. Trends in predicted N(V), N(-III), S(VI), EC, and OC concentrations illustrate the same effects.

Airborne PM has been identified as a significant threat to public health. Exposure assessment to ambient PM is essential for policy makers to develop appropriate and efficient risk reduction measures. Population-weighted exposure (PWE) can be used to estimate the average PM exposure in a study region. PWE is calculated as follows:

$$PWE = \frac{\sum_i C_i \times P_i}{\sum_i P_i} \quad (1)$$

where *i* is the grid point, *C<sub>i</sub>* is the concentration and *P<sub>i</sub>* the population density in grid cell *i*. Fig. 7 shows the estimated PWE to PM<sub>2.5</sub> mass and its components in the SJV based on the concentrations predicted using the three sets of meteorological fields. Predicted PWE to PM<sub>2.5</sub> mass is 52, 40, and 32 μg m<sup>-3</sup> when using

the DIA and WRF-FDDA, and WRF meteorological fields, respectively. The DIA and WRF-FDDA predictions suggest that the average person in the SJV experiences concentrations in excess of the 24-h average PM<sub>2.5</sub> National Ambient Air Quality Standard (NAAQS) of 35 μg m<sup>-3</sup>. In contrast, the air quality predictions made using the WRF meteorological fields do not result in PWE greater than the PM<sub>2.5</sub> NAAQS. It is expected that the diagnostic results are most accurate for sub-regions that contain the greatest number of meteorological measurements. This usually corresponds to urban areas that also experience the highest pollutant exposures. Diagnostic models are therefore weighted towards maximum accuracy in the most highly populated regions.

### 5. Sensitivity analysis

Different data products can be used for FDDA leading to different WRF predictions. In the present study, a sensitivity check was conducted using the 32 km North American Regional Reanalysis (NARR) dataset for WRF FDDA. The average surface temperature, relative humidity, U wind velocity, and V wind velocity in the SJV changed by 10.3%, -1.1%, -3.4%, and 5.7%, respectively, compared to the corresponding values produced using NCAR global reanalysis data. The population-weighted average exposure to total PM<sub>2.5</sub> changed by only +0.5 μg m<sup>-3</sup> (+1.2%) when NARR data was used, emphasizing the fact that the choice of the dataset used for WRF FDDA does not explain the large difference between the diagnostic and prognostic pollution predictions in the current study. We believe that the fundamental failure to predict the severe wind shear that was observed during the winter stagnation events

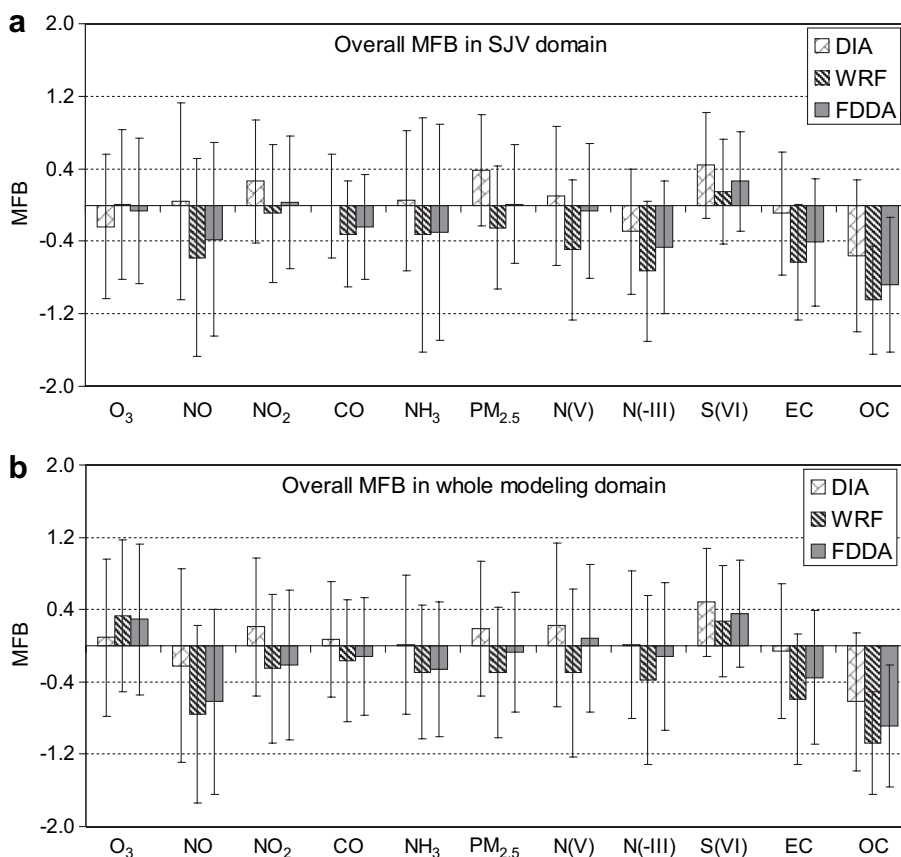
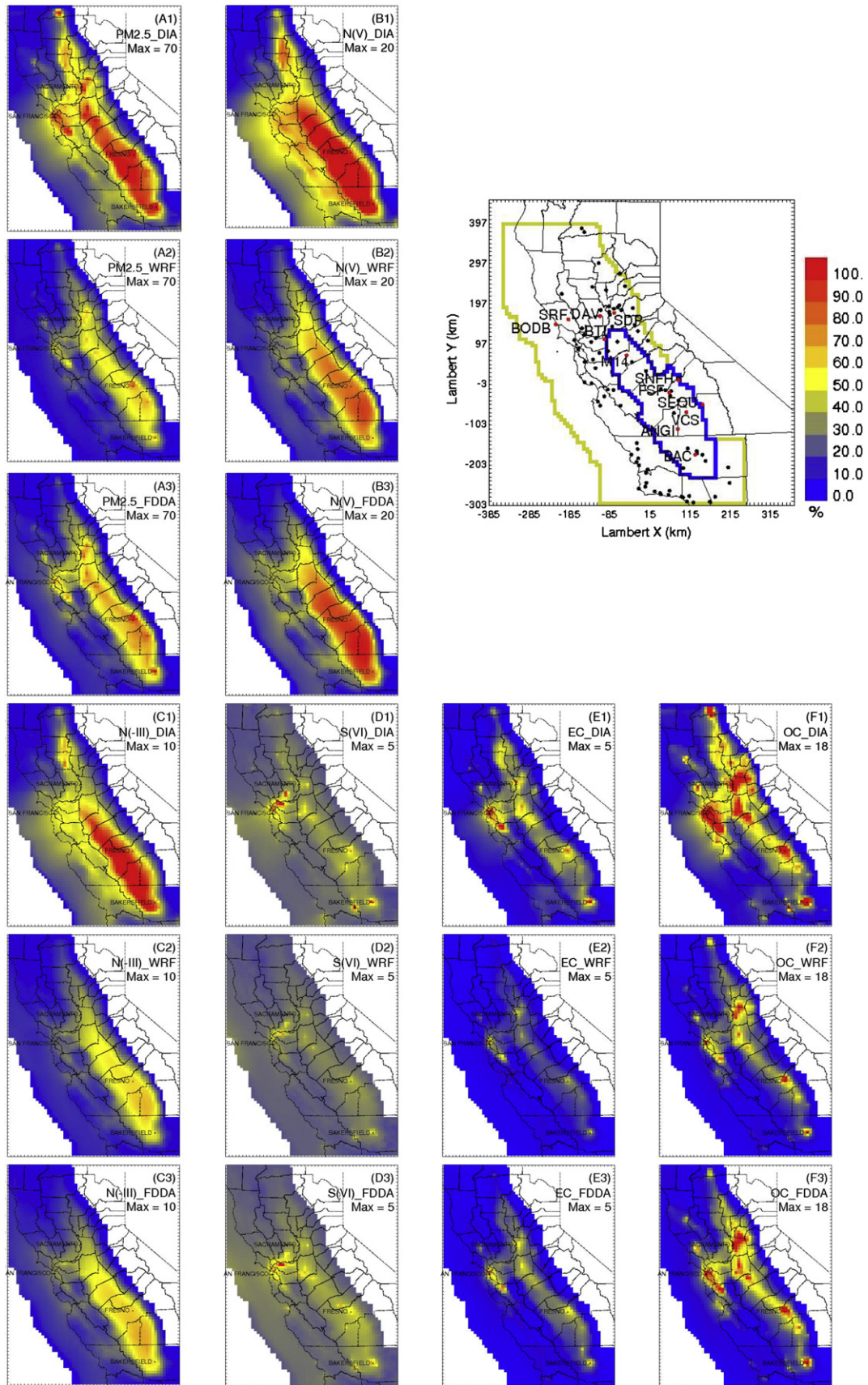


Fig. 5. Overall mean fractional bias calculated using all available observations for PM and gas species in (a) the SJV and (b) the entire modeling domain. Error bars represent the standard deviations of MFBs.



**Fig. 6.** Comparison of (A) PM<sub>2.5</sub>, (B) N(V), (C) N(-III), (D) S(VI), (E) EC, and (F) OC predicted with (1) diagnostic (DIA), (2) WRF-simulated (WRF), and (3) WRF-simulated with FDDA (FDDA) meteorological fields. All concentrations are expressed as % of the maximum value shown in each sub-panel. Absolute units are ppb for gas species and  $\mu\text{g m}^{-3}$  for PM species. The % scale is shown in the domain sub-panel (upper right corner) along with the active computational region (light yellow line) and the SJV (dark blue line). The dots represent the air quality sites used to evaluate model performance.

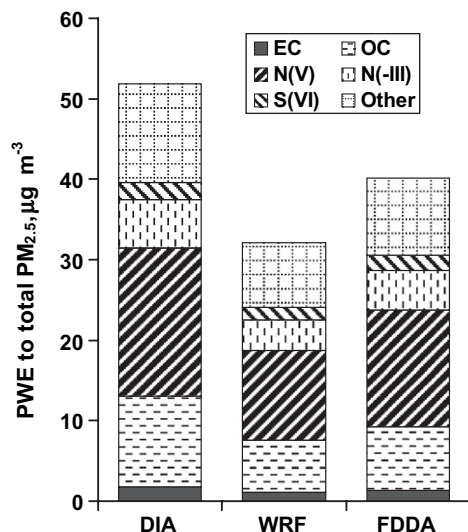


Fig. 7. Population-weighted exposure to PM<sub>2.5</sub>, EC, OC, N(V), N(-III), and S(VI) in the SJV predicted with (1) diagnostic (DIA), (2) WRF-simulated, and (3) WRF-FDDA simulated (FDDA) meteorological fields.

in California is a shortcoming of the WRF model itself, not the datasets used to drive the WRF model.

The nudging coefficients used with FDDA also affect the WRF meteorological fields and consequently the air quality predictions. Choi et al. (2009) studied the impact of the nudging coefficient on MM5 meteorological fields and ozone predictions, and found that larger nudging coefficients improve the model performance under asynoptic conditions but had little effect under synoptic conditions. A sensitivity test was conducted using a larger WRF-FDDA nudging coefficient of  $8 \times 10^{-4} \text{ s}^{-1}$  (vs. the base-case value of  $6 \times 10^{-4} \text{ s}^{-1}$ ) in the current study. The average temperature, relative humidity, U wind speed and V wind speed predicted in the SJV changed by 1.0%, -0.3%, -3.4%, and 2.9%, respectively, compared to the base-case FDDA results. Population-weighted average exposure to total PM<sub>2.5</sub> in the SJV decreased by  $0.7 \mu\text{g m}^{-3}$  (-1.7%) when the larger nudging factor was used. Once again, this change is small relative to the differences between the diagnostic and prognostic simulations in the current study.

## 6. Conclusions

The UCD/CIT air quality model was applied with three sets of meteorological fields to produce three sets of predictions for air pollutant concentrations during the CRPAQS 2000 winter episode in the San Joaquin Valley. The first set of meteorological fields was generated using a diagnostic model based on measured parameters combined with an objective analysis method. The second set of meteorological inputs was generated using WRF V2.2 prognostic model (no data nudging), and the third set was generated using WRF model with the FDDA technique. Statistical analysis of the predicted and measured meteorological time series shows that the WRF prognostic model does not accurately simulate stagnant wintertime meteorological temperature and wind fields in central California unless it is applied with FDDA. The combination of WRF-FDDA fields with air quality calculations improves air quality predictions during this episode. Diagnostic meteorological fields produced more accurate air quality predictions than prognostic fields overall during stagnant winter conditions. The overall MFB values of all pollutants produced by the diagnostic meteorological fields are within  $\pm 0.3$ , except for S(VI) MFB = 0.48 and OC MFB = -0.62. Population-weighted average PM<sub>2.5</sub> exposure is 40%

higher using diagnostic meteorological fields compared to prognostic meteorological fields created without data assimilation. The results indicate that meteorological fields generated by diagnostic methods based on a dense measurement network are the preferred choice for air quality model studies during stagnant periods in locations with complex topography such as California. Improvements to prognostic meteorological models, especially a better description of nocturnal ground-level inversions and small-scale dynamics (e.g., land-sea breezes and orographical winds), are needed to generate more accurate meteorological fields under these conditions.

## Acknowledgement

This research was supported by the San Joaquin Valleywide Air Pollution Study Agency under contract 2000-05PM. The statements, opinions, findings, and conclusions of this paper are those of the authors and do not necessarily represent the views of the California Air Resources Board. Further support was provided by the University of California Toxic Substances Research and Teaching Program (TSR&TP) through the Atmospheric Aerosols and Health Lead Campus Program (aah.ucdavis.edu).

## References

- Boylan, J.W., Russell, A.G., 2006. PM and light extinction model performance metrics, goals, and criteria for three-dimensional air quality models. *Atmospheric Environment* 40, 4946–4959.
- Byun, D.W., 1999. Dynamically consistent formulations in meteorological and air quality models for multiscale atmospheric studies. Part II: mass conservation issues. *Journal of the Atmospheric Sciences* 56, 3808–3820.
- Chen, F., Dudhia, J., 2001. Coupling an advanced land-surface/hydrology model with the Penn State/NCAR MM5 modeling system. Part I: model description and implementation. *Monthly Weather Review* 129, 569–585.
- Chen, J., Ying, Q., Kleeman, M.J. Source apportionment of wintertime secondary organic aerosol during the California Regional PM<sub>10</sub>/PM<sub>2.5</sub> Air Quality Study. *Atmospheric Environment*, in press. doi:10.1016/j.atmosenv.2009.07.010.
- Choi, H.J., Lee, H.W., Sung, K.H., Kim, M.J., Kim, Y.K., Jung, W.S., 2009. The impact of nudging coefficient for the initialization on the atmospheric flow field and the photochemical ozone concentration of Seoul, Korea. *Atmospheric Environment* 43, 4124–4136.
- Fountoukis, C., Nenes, A., 2007. ISORROPIA II: a computationally efficient thermodynamic equilibrium model for  $\text{K}^+\text{Ca}^{2+}\text{Mg}^{2+}\text{NH}_4^+\text{Na}^+\text{SO}_4^{2-}\text{NO}_3^-\text{Cl}^-\text{H}_2\text{O}$  aerosols. *Atmospheric Chemistry and Physics* 7, 4639–4659.
- Garratt, J.R., 1994. *The Atmospheric Boundary Layer*. Cambridge University Press, p. 155.
- Goodin, W.R., McRae, G.J., Seinfeld, J.H., 1979. Comparison of interpolation methods for sparse data – application to wind and concentration fields. *Journal of Applied Meteorology* 18, 761–771.
- Goodin, W.R., McRae, G.J., Seinfeld, J.H., 1980. Objective analysis technique for constructing 3-dimensional urban-scale wind fields. *Journal of Applied Meteorology* 19, 98–108.
- Grell, A.G., Dudhia, J., Stauffer, D.R., June 1994. A Description of the Fifth-Generation Penn State/NCAR Mesoscale Model (MM5). *NCAR Technical Note NCAR/TN-398+STR*. National Center for Atmospheric Research, Boulder, CO.
- Hanna, S.R., Moore, G.E., Fernau, M.E., 1996. Evaluation of photochemical grid models (UAM-IV, UAM-V, and the ROM/UAM-IV couple) using data from the Lake Michigan Ozone Study (LMOS). *Atmospheric Environment* 30, 3265–3279.
- Harley, R.A., Russell, A.G., McRae, G.J., Cass, G.R., Seinfeld, J.H., 1993. Photochemical modeling of the Southern California Air-Quality Study. *Environmental Science & Technology* 27, 378–388.
- Hass, H., Buitjes, P.J.H., Simpson, D., Stern, R., 1997. Comparison of model results obtained with several European regional air quality models. *Atmospheric Environment* 31, 3259–3279.
- Held, T., Ying, Q., Kaduwela, A., Kleeman, M., 2004. Modeling particulate matter in the San Joaquin Valley with a source-oriented externally mixed three-dimensional photochemical grid model. *Atmospheric Environment* 38, 3689–3711.
- Hogrefe, C., Rao, S.T., Kasibhatla, P., Hao, W., Sista, G., Mathur, R., McHenry, J., 2001a. Evaluating the performance of regional-scale photochemical modeling systems: part II – ozone predictions. *Atmospheric Environment* 35, 4175–4188.
- Hogrefe, C., Rao, S.T., Kasibhatla, P., Kallos, G., Tremback, C.J., Hao, W., Olerud, D., Xiu, A., McHenry, J., Alapaty, K., 2001b. Evaluating the performance of regional-scale photochemical modeling systems: part I – meteorological predictions. *Atmospheric Environment* 35, 4159–4174.
- Hong, S.Y., Noh, Y., Dudhia, J., 2006. A new vertical diffusion package with an explicit treatment of entrainment processes. *Monthly Weather Review* 134, 2318–2341.

- Hu, Y.T., Odman, M.T., Russell, A.G., 2006. Mass conservation in the Community Multiscale Air Quality model. *Atmospheric Environment* 40, 1199–1204.
- Jackson, B., Chau, D., Gurer, K., Kaduwela, A., 2006. Comparison of ozone simulations using MM5 and CALMET/MM5 hybrid meteorological fields for the July/August 2000 CCOS episode. *Atmospheric Environment* 40, 11.
- Jacobson, M.Z., 2005. A solution to the problem of nonequilibrium acid/base gas–particle transfer at long time step. *Aerosol Science and Technology* 39, 92–103.
- Jiang, G.F., Fast, J.D., 2004. Modeling the effects of VOC and NO<sub>x</sub> emission sources on ozone formation in Houston during the TexAQS 2000 field campaign. *Atmospheric Environment* 38, 5071–5085.
- Jimenez, P., Jorba, O., Parra, R., Baldasano, J.M., 2006. Evaluation of MM5-EM1-CAT2000-CMAQ performance and sensitivity in complex terrain: high-resolution application to the northeastern Iberian Peninsula. *Atmospheric Environment* 40, 5056–5072.
- Kleeman, M.J., Cass, G.R., 2001. A 3D Eulerian source-oriented model for an externally mixed aerosol. *Environmental Science & Technology* 35, 4834–4848.
- Kleeman, M.J., Cass, G.R., Eldering, A., 1997. Modeling the airborne particle complex as a source-oriented external mixture. *Journal of Geophysical Research-Atmospheres* 102, 21355–21372.
- Kleeman, M.J., Ying, Q., Lu, J., Mysliwicz, M.J., Griffin, R.J., Chen, J.J., Clegg, S., 2007. Source apportionment of secondary organic aerosol during a severe photochemical smog episode. *Atmospheric Environment* 41, 576–591.
- Kumar, N., Russell, A.G., 1996. Comparing prognostic and diagnostic meteorological fields and their impacts on photochemical air quality modeling. *Atmospheric Environment* 30, 1989–2010.
- Lee, S.M., Yoon, S.C., Byun, D.W., 2004. The effect of mass inconsistency of the meteorological field generated by a common meteorological model on air quality modeling. *Atmospheric Environment* 38, 2917–2926.
- Liang, J.Y., Martien, P.T., Soong, S., Tanrikulu, S., 2004. A photochemical model comparison study: CAMx and CMAQ performance in central California. In: *Proceedings of the Thirteenth Conference on the Application of Air Pollution Meteorology with the Air and Waste Management Association*, Vancouver, Canada. American Meteorological Society, Boston.
- McRae, G.J., Goodin, W.R., Seinfeld, J.H., 1982. Development of a 2nd-generation mathematical-model for urban air-pollution. 1. Model formulation. *Atmospheric Environment* 16, 679–696.
- Menut, L., Coll, I., Cautenet, S., 2005. Impact of meteorological data resolution on the forecasted ozone concentrations during the ESCOMPTE IOP2a and IOP2b. *Atmospheric Research* 74, 139–159.
- Mysliwicz, M.J., Kleeman, M.J., 2002. Source apportionment of secondary airborne particulate matter in a polluted atmosphere. *Environmental Science & Technology* 36, 5376–5384.
- Nenes, A., Pandis, S.N., Pilinis, C., 1998. ISORROPIA: a new thermodynamic equilibrium model for multiphase multicomponent inorganic aerosols. *Aquatic Geochemistry* 4, 123–152.
- Noilhan, J., Planton, S., 1989. A simple parameterization of land surface processes for meteorological models. *Monthly Weather Review* 117, 536–549.
- Odman, M.T., Russell, A.G., 2000. Mass conservative coupling of non-hydrostatic meteorological models with air quality models. In: Gryning, S.E., Batchvarova, E. (Eds.), *Air Pollution Modeling and its Application XIII*. Kluwer/Plenum, New York, pp. 651–660.
- Pielke, R.A., Cotton, W.R., Walko, R.L., Tremback, C.J., Lyons, W.A., Grasso, L.D., Nicholls, M.E., Moran, M.D., Wesley, D.A., Lee, T.J., Copeland, J.H., 1992. A comprehensive meteorological modeling system – RAMS. *Meteorology and Atmospheric Physics* 49, 69–91.
- Pun, B.K., Balmori, R.T.F., Seigneur, C., 2009. Modeling wintertime particulate matter formation in central California. *Atmospheric Environment* 43, 402–409.
- Seaman, N.L., 2000. Meteorological modeling for air-quality assessments. *Atmospheric Environment* 34, 2231–2259.
- Seaman, N.L., 2003. Future directions of meteorology related to air-quality research. *Environment International* 29, 245–252.
- Skamarock, W.C., Klemp, J.B., 2008. A time-split nonhydrostatic atmospheric model for weather research and forecasting applications. *Journal of Computational Physics* 227, 3465–3485.
- Skamarock, W.C., Klemp, J.B., Dudhia, J., Frill, D.O., Barker, M., Wang, W., Powers, J.G., 2005. A description of the advanced research WRF version 2. *NCAR Technical Note NCAR/TN-4688+STR*.
- Sistla, G., Hao, W., Ku, J.Y., Kallos, G., Zhang, K.S., Mao, H.T., Rao, S.T., 2001. An operational evaluation of two regional-scale ozone air quality modeling systems over the eastern United States. *Bulletin of the American Meteorological Society* 82, 945–964.
- Soong, S., Tanrikulu, S., Wilczak, J., Bao, J., Martin, P., Michelson, S., 2004. Simulation of an ozone episode during the Central California Ozone Study. Part II: CAMx air quality model simulations. In: *Proceedings of the Thirteenth Conference on the Application of Air Pollution Meteorology with the Air and Waste Management Association*, Vancouver, Canada. American Meteorological Society, Boston.
- Sportisse, B., Quelo, D., Mallet, V., 2007. Impact of mass consistency errors for atmospheric dispersion. *Atmospheric Environment* 41, 6132–6142.
- Stauffer, D.R., Seaman, N.L., 1990. Use of four-dimensional data assimilation in a limited area mesoscale model. Part I: experiments with synoptic-scale data. *Monthly Weather Review* 118, 1250–1277.
- Stauffer, D.R., Seaman, N.L., Binkowski, F.S., 1991. Use of four-dimensional data assimilation in a limited-area mesoscale model. Part II: effects of data assimilation within the planetary boundary layer. *Monthly Weather Review* 119, 734–754.
- Stauffer, D.R., Seaman, N.L., 1994. Multiscale four-dimensional data assimilation. *Journal of Applied Meteorology* 33, 416–434.
- Thompson, G., Rasmussen, R.M., Manning, K., 2004. Explicit forecasts of winter precipitation using an improved bulk microphysics scheme. Part I: description and sensitivity analysis. *Monthly Weather Review* 132, 519–542.
- Ying, Q., Fraser, M.P., Griffin, R.J., Chen, J.J., Kleeman, M.J., 2007. Verification of a source-oriented externally mixed air quality model during a severe photochemical smog episode. *Atmospheric Environment* 41, 1521–1538.
- Ying, Q., Kleeman, M.J., 2003. Effects of aerosol UV extinction on the formation of ozone and secondary particulate matter. *Atmospheric Environment* 37, 5047–5068.
- Ying, Q., Kleeman, M.J., 2006. Source contributions to the regional distribution of secondary particulate matter in California. *Atmospheric Environment* 40, 736–752.
- Ying, Q., Lu, J., Allen, P., Livingstone, P., Kaduwela, A., Kleeman, M., 2008. Modeling air quality during the California Regional PM<sub>10</sub>/PM<sub>2.5</sub> Air Quality Study (CRPAQS) using the UCD/CIT source-oriented air quality model – part I. Base case model results. *Atmospheric Environment* 42, 8954–8966.
- Zhan, Z., Chen, S., et al., Dynamically downscaling PCM with WRF for climate change impact in California: part I. Present time simulation analysis. *Journal of Climate*, in preparation.